Mass transfer limitations in binderless ZSM-5 zeolite granules during adsorption of flavour compounds from aqueous streams

Gernat, Deborah C.; Rozenbroek, Renzo; Brouwer, Eric R.; van der Wielen, Luuk A.M.; Ottens, Marcel

DOI
10.1002/jctb.6491

Publication date
2020

Document Version
Final published version

Published in
Journal of Chemical Technology and Biotechnology

Research Article

Received: 4 March 2020 Revised: 10 May 2020 Accepted article published: 21 May 2020 Published online in Wiley Online Library:

(wileyonlinelibrary.com) DOI 10.1002/jctb.6491

Mass transfer limitations in binderless ZSM-5 zeolite granules during adsorption of flavour compounds from aqueous streams

Deborah C Gernat,[a] Renzo Rozenbroek,[a] Eric R Brouwer,[b] Luuk AM van der Wielen[a,c] and Marcel Ottens[a]*

Abstract

BACKGROUND: Recently, a new process concept has been proposed to selectively adsorb wort off-flavours, *i.e.* aldehydes, from alcohol-free beers with hydrophobic zeolites.

RESULTS: In this work, we investigated the uptake of a mixture of wort flavour compounds (2-methylpropanal, 2-methylbutanal, 3-methylbutanal, furfural, and methional), from a model solution onto binderless hydrophobic ZSM-5 zeolite granules in order to quantify mass transfer parameters and identify bottlenecks. Subsequently, the homogenous solid diffusion model was employed to regress the effective diffusion coefficients for each molecule and experimental condition, which ranged between 10^{-15} and 10^{-13} m^2 s^{-1}, indicating strong intraparticle mass transfer limitation. Furthermore, it was found that the effective diffusion coefficient is inversely correlated to the molecules' hydrophobicity, expressed as the logD value and its isotherm affinity constant.

CONCLUSION: These results give valuable insight to design and improve the adsorbent material and an off-flavour removal unit at industrial scale.

Keywords: zeolites; adsorption; mass transfer; diffusion; downstream; removal

NOMENCLATURE

Symbol	Meaning/ SI units
A_s	External surface area of adsorbent granules [m^2]
Bi	Biot number []
c	Concentration in the bulk liquid [mol m^{-3}] or [kg/kg]
c_s	Concentration at the surface [mol m^{-3}]
C	Brunauer–Emmett–Teller (BET) constant []
D_c	Intracrystalline diffusivity [m^2 s^{-1}]
d_c /d_p	Crystal/particle diameter [m]
D_{eff}	Effective diffusivity [m^2 s^{-1}]
d_{extr}	Diameter extrudate [m]
D_L	Axial dispersion [m^2 s^{-1}]
D_m	Molecular diffusivity in water [m^2 s^{-1}]
D_{macro}	Macropore diffusivity [m^2 s^{-1}]
J	Flux [mol s^{-1} m^{-2}]
K	Adsorption equilibrium constant []
k_{eff}	Overall mass transfer coefficient [s^{-1}]
k_f	Film mass transfer coefficient [m s^{-1}]
K_F	Adsorption equilibrium constant Freundlich model (unit variable)
M	Molecular weight [kg mol^{-1}]
m	Mass [kg]
n	Adsorption equilibrium constant Freundlich model (unit variable)
p / p^o	Pressure / saturation vapour pressure [kg·m^{-1} s^{-2}]
Q	Quantity (unit variable)
q_e	Loading of adsorbent at equilibrium [mol kg^{-1}] or [kg/kg]
q_t	Loading of adsorbent at time t [kg/kg]
q_p	Loading at pressure p [mol kg^{-1}]
q_{mono}	Loading at monolayer coverage [mol kg^{-1}]
r_p / r_c	Radius of particle / crystal [m]
t	Time [s]
T	Temperature [K]
u	Interstitial velocity [m s^{-1}]

* Correspondence to: M Ottens, Department of Biotechnology, Delft University of Technology, van der Maasweg 9, 2629 HZ Delft, The Netherlands, E-mail: *m.ottens@tudelft.nl*

a *Department of Biotechnology, Delft University of Technology, Delft, The Netherlands*

b *Heineken Supply Chain, Global Innovation & Research, Zoeterwoude, The Netherlands*

c *Bernal Institute, University of Limerick, Castletroy, Co, Limerick, Ireland*

V_b	Liquid bulk volume [m^3]
V_m	Molecular volume [m^3]
ε	Particle porosity []
η	Viscosity [kg /(m· s^2)]
ρ	Density [kg m^{-3}]
ξ	Eigenvalue of Bessel function []
σ	Standard deviation (unit variable)
σ_m	Standard error (unit variable)
τ	Tortuosity []
Ψ	Constant solute-solvent interaction []

ABBREVIATIONS

2-MB	2-Methylbutanal
2-MP	2-Methylpropanal
3-MB	3-Methylbutanal
ARE	Average relative error
BEA	Zeolite framework type (beta)
EDX	Energy dispersive X-ray
FAU	Zeolite framework type (faujasite)
FF	Furfural
HSDM	Homogeneous surface diffusion model
Met	Methional
R^2	Coefficient of determination
SEM	Scanning electron microscope
ZSM-5	Zeolite Socony Mobil-5

INTRODUCTION

Mass transfer during gas adsorption in microporous materials has been widely studied.[1–4] Fewer studies are available investigating mass transfer in shaped microporous materials in liquids, and more specifically, aggregated pellets or granules in dilute aqueous environments. Even so, new applications of zeolites in aqueous systems are emerging. For instance, waste water treatment,[5–7] or the separation and conversion of sugars, has been investigated in the past.[8–12] In the production of biofuels, zeolites have also been employed to optimize production.[13, 14] In a recent study, a new technology has been developed to selectively remove off-flavours from complex aqueous food streams, in particular wort flavour from alcohol-free beer with ZSM-5 type zeolites.[15] Wort flavour compounds, namely (Strecker) aldehydes, are often present in elevated concentrations, which distorts the sensory perception of the product. The most dominant contributors to the wort flavour are 2-methylbutanal (2-MB), 3-methylbutanal (3-MB), and methional (Met),[16, 17] as well as 2-methylpropanal (2-MP).[18] Furthermore, furfural (FF), as a general indicator for flavour instability,[19] is of interest in this study. The authors reported that separation based on hydrophobicity and size exclusion ensured a high selectivity and capacity. Hydrophobic ZSM-5 type zeolites (SiO_2/Al_2O_3 molar ratio 360) proved to be particularly promising to target unwanted aldehydes while retaining major contributors to the flavour of the beer, such as hop and small organic acids in the product.[15] In order to show the technical and, ultimately, economic feasibility of such a technology, the mass transfer in such a multicomponent system needs to be studied and characterized thoroughly.

Previous work has mainly focused on studying the mass transfer in single component systems, *e.g.* sugar molecules in aqueous solutions,[20–26] simple alcohols, ketones, and aromatics[27, 28] or amino acids.[29] Relevant data is summarized in Table 1. The reported diffusivities range vastly, from $8.0{\cdot}10^{-17}$ to $2.4{\cdot}10^{-11}$ m^2s^{-1}. Most commonly, a simplified equation of the homogenous solid diffusion model (HSDM) is employed to regress the diffusivity, but the table also illustrates that simplifications and assumptions of different mass transfer models are applied, potentially leading to different results. This makes a comparison, even in the order of magnitude, rather difficult.

The objective of this work is to quantify mass transfer parameters and identify possible bottlenecks for mass transportation in the zeolite. In addition, a better understanding of the main impact factors on transport is gained. This may lead to more insight for designing an adsorbent material with improved mass transfer properties. Furthermore, the data can be implemented in process simulations for the conceptual design of an adsorptive off-flavour removal unit. To do so, the structural properties of the solid adsorbent were studied first to obtain insight into the macro- and microstructure of the material. Then, the adsorption process dynamics were determined during hydrodynamically defined batch uptake experiments, varying the particle size of the ZSM-5 G-360 granules, as well as the solute starting concentrations. Subsequently, the HSDM was employed to regress effective diffusion coefficients, which were then correlated to the respective molecular properties.

THEORY

Isotherm model

The equilibrium isotherms of the tested solutes were regressed from experimental adsorption data with the Freundlich isotherm model, according to equation (1).[30] If *n* converges towards one, the equation equals the linear adsorption model isotherm and the assumptions of a non-competitive adsorption process can be considered within the defined experimental design space, making a multicomponent isotherm model obsolete.

$$q_{e,i} = K_F \cdot c_{e,i}^{1/n} \tag{1}$$

Adsorption model

In principle, there are two types of microporous adsorbents: homogenous particles, which exhibit a wide pore size distribution; and composite pellets, which consist of microparticles (crystals) shaped into the desired form and often show a well-defined bimodal pore size distribution.[31] In the latter case, micropores and meso/macropores can be clearly distinguished. Both pore type diffusivities can be limiting, depending on the conditions and the system. Hence, mass transfer is classified into: (i) liquid film diffusion; and (ii) intraparticle diffusion, consisting of diffusion through the macro- and micropores (as seen in Fig. 1(a)). While within the macropore, two transport mechanisms are possible, *i.e.* pore diffusion through the liquid and surface diffusion along the solid adsorbent surface, the transport in the micropores of the crystals is limited to intracrystalline diffusion, which resembles surface diffusion in the mechanism.[32] In addition to the above explained transport mechanisms, surface barriers, *e.g.* at the particle shell or the crystal surface, may occur and impact the sorption dynamics.[31, 33–35] Since mass action is a very rapid process in physiosorption, it is neglected and hence, either film or intraparticle diffusion always is the rate limiting step.[31]

For this work, we created experimental conditions to eliminate external mass transfer conditions as much as possible in order to measure the intraparticle diffusivity. The film mass transfer

Journal of Chemical Technology & Biotechnology published by John Wiley & Sons Ltd on behalf of Society of Chemical Industry.

Table 1 Relevant diffusion coefficients for small molecules in aqueous solutions into zeolites as reported in literature

Adsorbent	Adsorbate	Adsorbent shape	Diameter	T [°C]	Mass transfer model	D [m^2s^{-1}]	
Silicalite	Methanol Ethanol Acetone	Powder	d_C = 1.2 µm	30	Direct time domain fitting of the liquid chromatography response peaks	$D_{c,\ MeOH} = 3.40{\cdot}10^{-14}$ $D_{c,\ EtOH} = 2.24{\cdot}10^{-14}$ $D_{c,\ AcO} = 2.04{\cdot}10^{-15}$	(27)
Hydrophocally modified NaY-zeolite	Benzene Toluene Ethylbenzene m,p-Xylene o-Xylene	Powder	n/a	28	HSDM	$D_{c,\ Benz} = 1.39{\cdot}10^{-13}$ $D_{c,Tol} = 1.11{\cdot}10^{-14}$ $D_{c,\ EtB} = 1.11{\cdot}10^{-14}$ $D_{c,\ mp} = 5.56{\cdot}10^{-14}$ $D_{c,\ Xyl} = 9.72{\cdot}10^{-14}$	(28)
FAU (Si/Al 150)	Isomaltotriose	Powder	d_c = 6 µm	5	Not specified	$D = 4{\cdot}10^{-13}$	(24)
BEA50	Isomaltose	Powder	d_c = 30 µm	30	Simplified HSDM regressing initial slope of uptake curve[1](52)	$D_c = 1.9{\cdot}10^{-12}$	(20)
BEA150 (extrudate of BEA50	Isomaltose	Extrudate	d_{extr} = 0.5 mm	30		$D_{ext} = 2.4{\cdot}10^{-11}$	
BEA50	Laminaribiose	Powder	d_C = 30 µm	40	Infinite bath solution of HSDM for cylindrical particles[2]	$D_c = 1.47{\cdot}10^{-14}$	(25)
BEA150	Laminaribiose	Extrudate	d_{extr} = 0.5 mm			$D_{ext} = 4.39{\cdot}10^{-11}$	
Hydrophobic Y-zeolite	Difructose dianhydrides	Powder	d_c = 6.6 µm	20-25	Long-term solution of HSDM (31)[3]	$D_c = 8{\cdot}10^{-17}$	(21)
Y-zeolite	Sucrose	Powder	dp = 6 µm	5	Micropore diffusion control (31)	$D_c = 1{\cdot}10^{-14}$	(22)
Hydrophilic KX-zeolite	Glucose Fructose Glycine Alanine Lysine	Powder	d_p = 50 µm	25	Extended van Deemter equation[4]	$D_c = 1.1{\cdot}10^{-13}$ $D_c = 1.3{\cdot}10^{-13}$ $D_{c,\ gly} = 1.9{\cdot}10^{-12}$ $D_{c,ala} = 7.2{\cdot}10^{-13}$ $D_{c,lys} = 1.8{\cdot}10^{-13}$	(26) (29)
Dealuminated, hydrophobic Y-zeolite	Glucose Sucrose	crushed granulated pellets	d_p = size 0.28 - 0.56 mm	20-25	Extended van Deemter equation[5]	$D_{c,\ glucose} = 2.1{\cdot}10^{-13}$ $D_{macro,\ glucose} = 1.4{\cdot}10^{-10}$ $D_{c,\ sucrose} = 1.0{\cdot}10^{-14}$ $D_{macro,\ sucrose} = 3.1{\cdot}10^{-10}$	(23)

[1] $\frac{q_t - q_0}{q_e - q_0} = \frac{2A}{V}\sqrt{\frac{D \cdot t}{\pi}}$

[2] $\frac{q_t}{q_{max}} = 1 - 4\sum_{n=1}^{\infty}\frac{1}{\xi_n^2}\exp\left(-\frac{\xi_n^2 Dt}{r^2}\right)$

[3] $q = 1 - \frac{6}{\pi^2}e^{\left(\frac{-\pi^2 D_c t}{r_c^2}\right)}$

[4] $\mathrm{HETP} \approx \frac{2D_L}{\nu} + \frac{2\varepsilon u}{(1-\varepsilon)}\left(\frac{1}{k_{eff}K}\right)\left(1 + \frac{\varepsilon}{(1-\varepsilon)K}\right)^{-2}$ with $\frac{1}{k_{eff}K} = \left(\frac{r^2}{15DK_c}\right)$

[5] with k_{eff} defined as $\frac{1}{k_{eff}K} = \frac{R_p^2}{15\varepsilon D_p} + \frac{R_c^2}{15KD_c}$ with $D_p = \frac{D}{\tau^2}$

coefficient, k_f, was calculated according to the widely accepted correlation given in Eqns (2) and (3).[30, 36, 37]

$$k_f = \sqrt{\frac{4D_m u}{\pi d_p}} \tag{2}$$

$$D_m = \frac{T}{\eta}7.4{\cdot}10^{-8}\frac{(\psi M)^{1/2}}{V_m^{0.6}} \tag{3}$$

In our case, granular particles of different diameters composed of small crystals are used. Such aggregated materials can be controlled by micropore or macropore diffusion or even by a mixed mechanism, where the adsorbate is transported through the relatively large macro- or mesopores by (fast) pore diffusion and then diffuses into the solid microporous crystals through slower intracrystalline diffusion. Although the studied material has a heterogeneous structure, the above explanation shows that the underlying mass transfer mechanisms can be complex and that simplifications to model the adsorption process are required. Such a model, commonly employed for representing intraparticle mass transfer in zeolites, is the homogenous solid diffusion model (HSDM),[38, 39] which is described through Eqn (4)–(6). The HSDM does not attempt to describe the adsorption process based on structural characteristics of the material, such as surface area or pore size (distribution), but rather as a simplified process, where the target compound adsorbs at the surface of the particle and then diffuses through it solely by means of solid diffusion. Thereby, the solid concentration profile is gradually decreasing

Journal of Chemical Technology & Biotechnology published by John Wiley & Sons Ltd on behalf of Society of Chemical Industry.

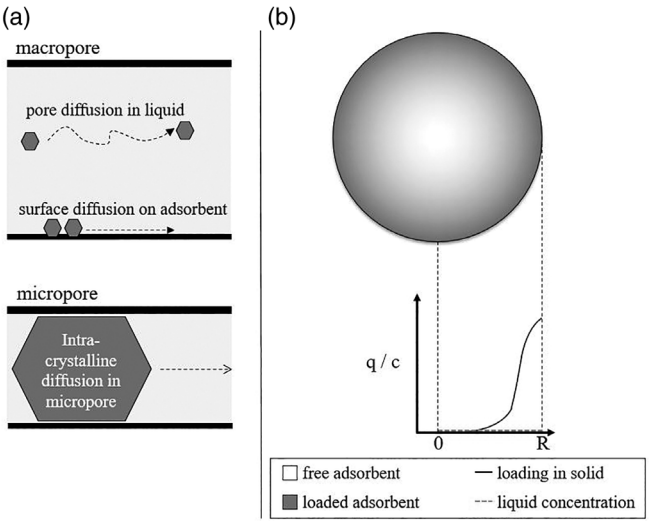

Figure 1 (A) Mechanisms of diffusion in macro- and micropores (B) schematic representation of the HSDM.

and the intraparticle sorbate concentration in the liquid phase equals zero, as shown in Fig. 1(b). This means, that the regressed diffusion coefficient is an effective one, rather than the specific diffusivity of the solute in the material.[40]

$$V_b \frac{\partial c_i}{\partial t} = -J_i A_S \tag{4}$$

$$J_i = k_f (c_i - c_{i,s}) \tag{5}$$

$$\frac{\partial q_i}{\partial t} = D_{eff}\left(\frac{\partial^2 q_i(r,t)}{\partial r^2} + \frac{2}{r}\frac{\partial q_i}{\partial r}\right) \tag{6}$$

The following assumptions are taken to simplify the system:

- Adsorbates do not interact with each other, only with the adsorbent.
- A non-competitive adsorption model (Freundlich) can describe the multicomponent equilibrium between the liquid and the solid according to Eqn (1).
- The HSDM assumes storage and transport of the sorbate only in the solid phase, making surface diffusion the predominant transport mechanism.
- The effective diffusivity is independent of the concentration.
- The experimental conditions are such that there is no concentration gradient over the column bed of adsorbent particles, so that the system can be modelled as an ideally mixed, finite bath.
- The average particle diameter of the granule is representative for the sample.

Equation (6) is solved with the boundary conditions defined in Eqns (7)–(9), meaning that there is no flux across the centre of the particle, and that the concentration of the bulk is c_0 at t = 0 and the initial loading of the solid is equal to zero.

$$\frac{\partial q_i(r=0,t)}{\partial r} = 0 \tag{7}$$

$$c_b(t=0) = c_0 \tag{8}$$

$$q_i(r,t=0) = 0 \tag{9}$$

Statistical analysis

The standard deviation of the sample σ was determined for the statistical deviations of the batch uptake experiment and the analytical measurement (shown in Eqn (10)). Furthermore, the systematic error of the calibration was considered. The propagated overall error of a quantity Q was then calculated from the standard error, σ_m, according to Eqns (11)–(12).[41]

$$\sigma = \sqrt{\frac{1}{(n-1)}\sum_{i=1}^{n}(x_i - \bar{x}^2)} \tag{10}$$

$$\sigma_m = \frac{\sigma}{\sqrt{n}} \tag{11}$$

$$\sigma_{mQ} = \sqrt{\sum_i \left(\frac{\partial Q}{\partial i}\right)^2 \sigma_{mi}^2} \tag{12}$$

The error of regressed parameters was determined from the variance–covariance matrix, calculated from the Jacobian of the fitting function.

MATERIALS AND METHODS

Materials

Solutions were prepared with milli-Q grade water (Merck Millipore, United States) or absolute ethanol (VWR International BV, The Netherlands). Maltodextrin type C*Dry MD 01958 was obtained from Cargill (Belgium) and phosphoric acid from J.T. Baker (The Netherlands). The binderless zeolite granules ZSM-5 G-360 were purchased from ACS Materials (United States). All other chemicals were purchased from Sigma Aldrich (The Netherlands).

Model solution

The physical properties and chemical composition of the model solution were chosen to resemble an alcohol-free beer. The viscosity was set to 2.8 mPa·s by adding 65 g L^{-1} maltodextrin. Maltodextrin was also chosen to represent the sugars contained in alcohol-free beers produced by arrested/restricted fermentation. The pH was adjusted to 4.2 by adding phosphoric acid. Depending on the experiment, either 0.5, 0.25, or 0.125 mg L^{-1} of each flavour compound (2-MP, 2-MB, 3-MB, FF and Met) dissolved in pure ethanol was added to the solution. The resulting ethanol content was 0.1 vol. %.

Adsorbent preparation

Zeolite granules were sieved into three different particle sizes (small 2.35 ± 0.11 mm; medium 2.66 ± 0.10 mm; large 3.12 ± 0.20 mm) or crushed with a mortar and pestle, with addition of a small amount of water to avoid dust formation. Before the experiments, granules were incubated overnight in 70% ethanol. Then the ethanol was removed via vacuum filtration and the particles were additionally washed with milli-Q grade water over the filter. After washing, the particles were dried overnight at 220 °C to remove all liquid and reach a stable dry weight.

Determination of material characteristics

Gravimetric method to determine porosity

To understand the accessibility of the particles to liquid, the volumetric update of water and ethanol-water mixtures was studied. First, the solid density was determined in a pycnometer. To do so, it was filled with dried adsorbent particles and the mass was

Journal of Chemical Technology & Biotechnology published by John Wiley & Sons Ltd on behalf of Society of Chemical Industry.

measured. Thereafter, it was filled with 20 v/v % ethanol and left to equilibrate. After topping the pycnometer with liquid, the weight was determined again. Knowing the density of the liquid, this allowed us to calculate the solid density according to Eqn (13). To calculate the porosity, the difference in adsorbent liquid and dry weight was determined with 70 v/v % ethanol and milli-Q grade water, respectively, and determined according to Eqns (14) and (15).

$$\rho_s = \frac{m_{ads,dry}}{V_{total} - V_{ethanol}} \tag{13}$$

$$V_{pore} = \frac{m_{ads,wet} - m_{ads,dry}}{\rho_l m_{ads,dry}} \tag{14}$$

$$\varepsilon_p = \frac{V_{pore}}{V_{pore} + V_{solid}} = \frac{V_{pore}}{V_{pore} + m_{ads}/\rho_{solid}} \tag{15}$$

Determination of pore size distribution by volumetric adsorption measurement with nitrogen

A defined amount of sample was degassed at 105 °C under vacuum prior to the measurement, yielding an approximate mass of 1.8 g of material for analysis. The sorption measurement of oxygen free nitrogen gas (B.O.C., United Kingdom) on ZSM-5 G-360 was carried out at −196 °C with a surface area and porosimetry analyser (ASAP 2420, Micrometrics, United States) using 40 adsorption and 30 desorption pressure points, respectively. Prior to the analysis, the sample was outgassed under a vacuum of 10 µmHg at 50 °C, and subsequently 110 °C, for 2 h. The corresponding isotherm was consequently analysed with the B.E.T. model,[42] assuming unrestricted multilayer formation according to Eqn (16). The measurement was carried out in duplicate. The calculation of the overall and the micropore volume was done with analysis software VersaWin (version 2.0) of Quantachrome Instruments.

$$\frac{p}{q_p(p^o - p)} = \frac{1}{q_{mono}C} + \frac{(C-1)}{q_{mono}C}\frac{p}{p^o} \tag{16}$$

Determination of pore size distribution by volumetric adsorption measurement with mercury

A defined amount of sample was conditioned for 6 h at 300 °C and analysed in a mercury porosimeter (Pascal 140 and 440, Porotech, Germany). The analysis was evaluated according to ISO 15901-1.[43]

Microscopic analysis

Microscopic pictures were taken with a light microscope from Leica type M202 FA (Germany) equipped with a digital camera (Leica DFC240) and a scanning electron microscope (SEM) EVO LS 25 (Zeiss, Germany). Additionally, samples were analysed with energy dispersive X-ray (EDX) of detector XFlash 5030 (BRUKER, United States).

Determination of multicomponent isotherm

To obtain multicomponent isotherms, simple batch uptake experiments were carried out with crushed zeolite particles. The pre-determined amount of adsorbent was weighed into a glass vial and the model solution was subsequently added by carefully pouring it into the vial. The vials were stirred overnight with a closed cap at 5 °C. An overview on the experiments performed to determine the isotherm is given in Table 4 in the appendix. All experiments were done in duplicate.

Hydrodynamically defined batch uptake experiments

Prior to the experiment, 1.5 g of washed and dried particles was incubated overnight in milli-Q grade water to ensure equilibration with the solvent. They were then packed into a glass column with a diameter of 1 cm and an adjustable length (Omnifit, USA), which was connected to a double-walled stirred reactor of 2 L capacity (Applikon, The Netherlands). The scheme of the set-up is shown in Fig. 2. Throughout the duration of the experiment, the temperature was controlled with a water bath at 5 °C and the system was kept closed to avoid losses due to evaporation. To start the experiment, the reactor was filled with 1.5 L model solution and stirred at 600 rpm. A blank sample was taken from the sample port and then, the model solution was circulated at a flow rate of 60 mL min^{-1}, resulting in a superficial velocity of 76.4 cm min^{-1}. The flow rate was chosen as such that the concentration gradient over the column, as well as external mass transfer limitations, were minimal to negligible (data shown in appendix material, Fig. 12). Samples were taken frequently during a period of 22.5 h to follow the uptake of aldehydes, and each experiment was carried out in duplicate to estimate the experimental error. Three different particle sizes were tested. In order to ensure that equilibrium can be reached, a prolonged batch of 54 hours was carried out in duplicate with particles of a diameter of 2.35 mm. The initial concentration of all five compounds of interested was set to $c_0 = 0.5$ mg/L.

Analysis of aldehydes

To analyse the concentration of aldehydes, samples were diluted with 65 g L^{-1} maltodextrin solution to the calibration range (<100 µg kg^{-1}) and were subsequently analysed by headspace solid-phase micro-extraction (HS-SPME) in a GC–MS (Agilent 7890A and 5975C MSD) and a 30 m x 0.25 mm x 0.25 µm 142 VF17MS column with an adapted protocol from Vesely *et al.* (2003).[44] The carrier gas (helium) was used at a flow rate of 1 mL min^{-1}. The calibration was performed by internal standard addition to increase the accuracy.

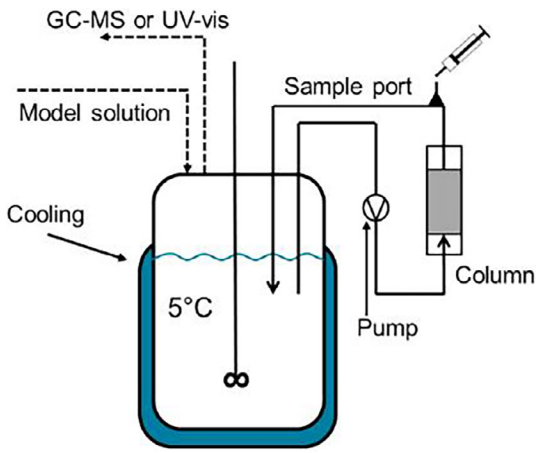

Figure 2 Schematic set-up for hydrodynamically defined batch uptake experiments.

Journal of Chemical Technology & Biotechnology published by John Wiley & Sons Ltd on behalf of Society of Chemical Industry.

Mathematical modelling

The model of the intraparticle mass transfer was built in COMSOL Multiphysics (version 5.3a) and the regression was performed by coupling the model to Matlab R2018b, to identify the optimal solution with *lsqcurvefit*, a nonlinear least-squares solver. Advanced Chemistry Development Inc. (ACD/Labs) software[45] was used to estimate the logD values and the molar volume.

RESULTS AND DISCUSSION

Adsorbent characterization

The general structure of ZSM-5 G-360 granules is depicted in the light microscope images in Fig. 3(a) and (b). The granules consist of small zeolite crystals pressed into a spherical shape in a kind of ring formation. The edge where breakage occurs is, hence, spherical as well. A closer look with SEM images in Fig. 3(c), (d) reveal a denser layer at the outer side of the particle, forming a shell around the granule for stability purposes. To understand the hierarchical structure of the material, further characterisation techniques were applied.

The analysis of the material by nitrogen adsorption (data in appendix) led to the following findings: as expected, the material exhibits a high micropore volume, caused by the ZSM-5 characteristic micropores of 5.4–5.6 Å. Small mesopores were found in the range of 2.0–3.0 nm, while pores >5 nm were absent. Since the hysteresis observed in the N_2 isotherm is relatively narrow, we can conclude that the pore size distribution is also well defined. Furthermore, the plateau of the isotherm indicates that there is only a small volume of mesopores present. This was confirmed by analyzing the respective pore volumes. After applying the Rouquerol correction, the micropore volume was determined with the t-plot method to 0.175 $cm^3\ g^{-1}$. The combined meso- and micropore volume was calculated to 0.195 $cm^3\ g^{-1}$, meaning that the resulting mesopores volume is approximately 0.020 $cm^3\ g^{-1}$.

Additionally, the porosity of larger pores in the range of ~10 nm – 100 µm was studied by mercury porosimetry. A distinct peak was found around ~180 nm. This suggests that the granule originally contained a binder that was removed during calcination, forming homogeneous macropores for transport of the adsorbate to the crystals, rather than being synthesized and grown from the seed. The macropore volume from the measurement amounted to 0.28 $cm^3\ g^{-1}$ and the mesopore volume (10–50 nm) to 0.015 $cm^3\ g^{-1}$. The mesopores volume is comparable to that found during N_2 sorption, however, in a higher pore size range. The mesopores pore volume of pores <10 nm is not evaluated, since the high applied pressure and potential destruction of the material structure could occur.

To determine the accessible volume for liquids, the porosity was also determined with a gravimetric method using ethanol as a sorbate. The solid density and porosity were averaged over all particle sizes, resulting in 2.23 ± 0.3 kg L^{-1} and 0.54 ± 0.2, respectively. The apparent particle density, hence, is 1.05 ± 0.04 kg L^{-1}. The same experiment carried out with water led to a 20% lower porosity, indicating that the granule is not fully accessible to the polar liquid. This observation was previously made by Wach *et al.* (2018), who found that the total porosity experimentally determined by the retention of D_2O was about 10% lower than the total porosity determined through N_2 and Hg porosimetry.[23] Assuming the same solid density, the porosity determined with the gravimetric method is compared to the porosity from N_2 and Hg adsorption. Here, a value of 0.51 is calculated, which is in agreement with the gravimetric value. The slightly higher value could be explained by the fact that microporosity is often underestimated by the t-plot method in hierarchical materials,[46] but experimental errors can also play a role. Because we are investigating the behaviour of organic compounds in a

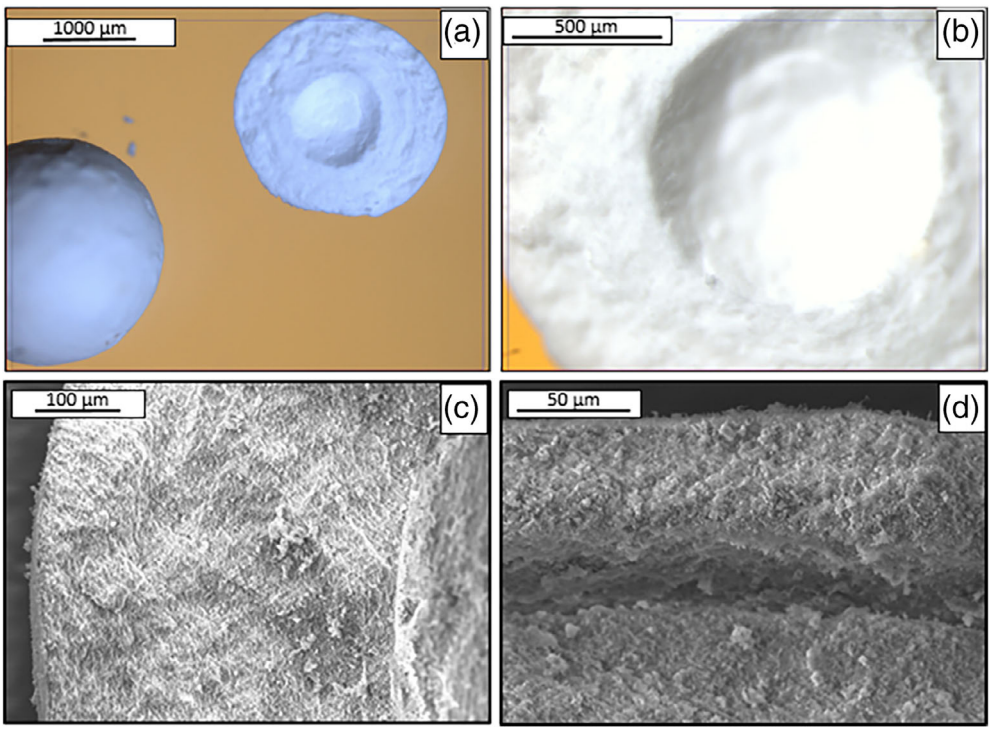

Figure 3 Light microscope images (top) and scanning electron microscopy picture of zeolite G-360 (c) core and (d) shell.

Journal of Chemical Technology & Biotechnology published by John Wiley & Sons Ltd on behalf of Society of Chemical Industry.

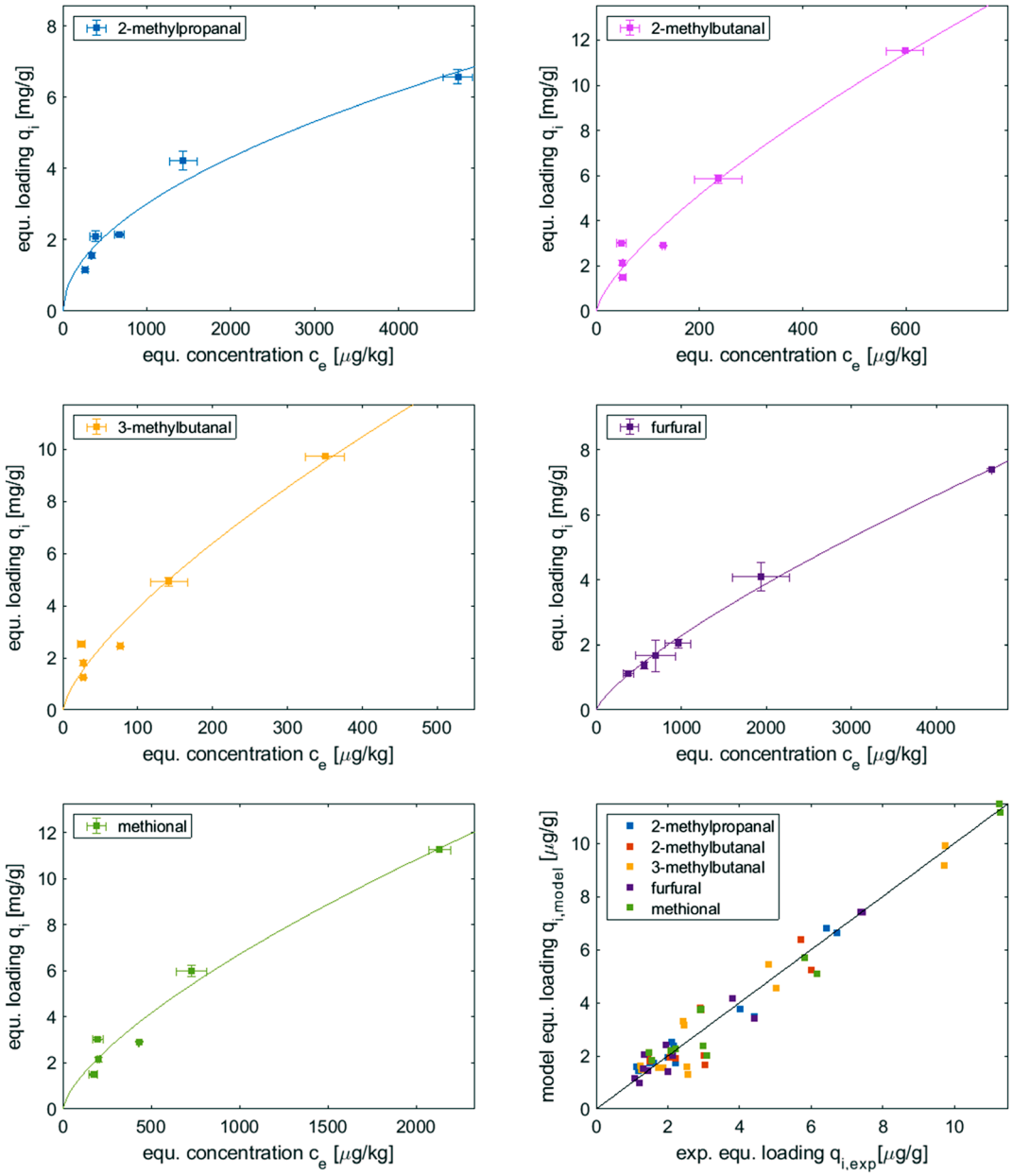

Figure 4 Freundlich isotherms and parity plot for all compounds of the model solution at pH 4.2.

liquid system, we consider the accessibility of the target molecules to the pores resemble most likely those of ethanol. We hence chose to base our proceeding analysis based on the results of the gravimetric method with water and ethanol.

Adsorption equilibrium

To be able to investigate the dynamics of the studied system, the equilibrium conditions, *i.e.* the adsorption isotherms, must be determined. Therefore, batch uptake experiments were performed at different compositions of the model solution. The results are plotted in Fig. 4. Generally, the equilibrium uptake can be characterized by the Freundlich isotherm with a slight decline in isotherm slope with increasing concentration. The parity plot confirms that the distribution is equally spread, and the model is a good representation of the experimental data. When regarding the affinities of the compounds to the adsorbent, one can find a relation between the hydrophobicity of the compound with the affinity to the adsorbent. This was also reported in previous research on alcohol-free beer.[15] 2- and 3-MB adsorb the strongest, followed by Met, while 2-MP and FF show the lowest adsorption loading under given conditions. Although there are multiple compounds in the system, we assume that the diffusivity can be regressed for a single compound. This is based on the following reasoning: (i) the system is very dilute ($c < 0.5$ mg L^{-1}); and (ii) the isotherms show a near linear behaviour in the observed range (<0.5 mg L^{-1}), hence, allowing the assumption of non-competitive adsorption process.

Journal of Chemical Technology & Biotechnology published by John Wiley & Sons Ltd on behalf of Society of Chemical Industry.

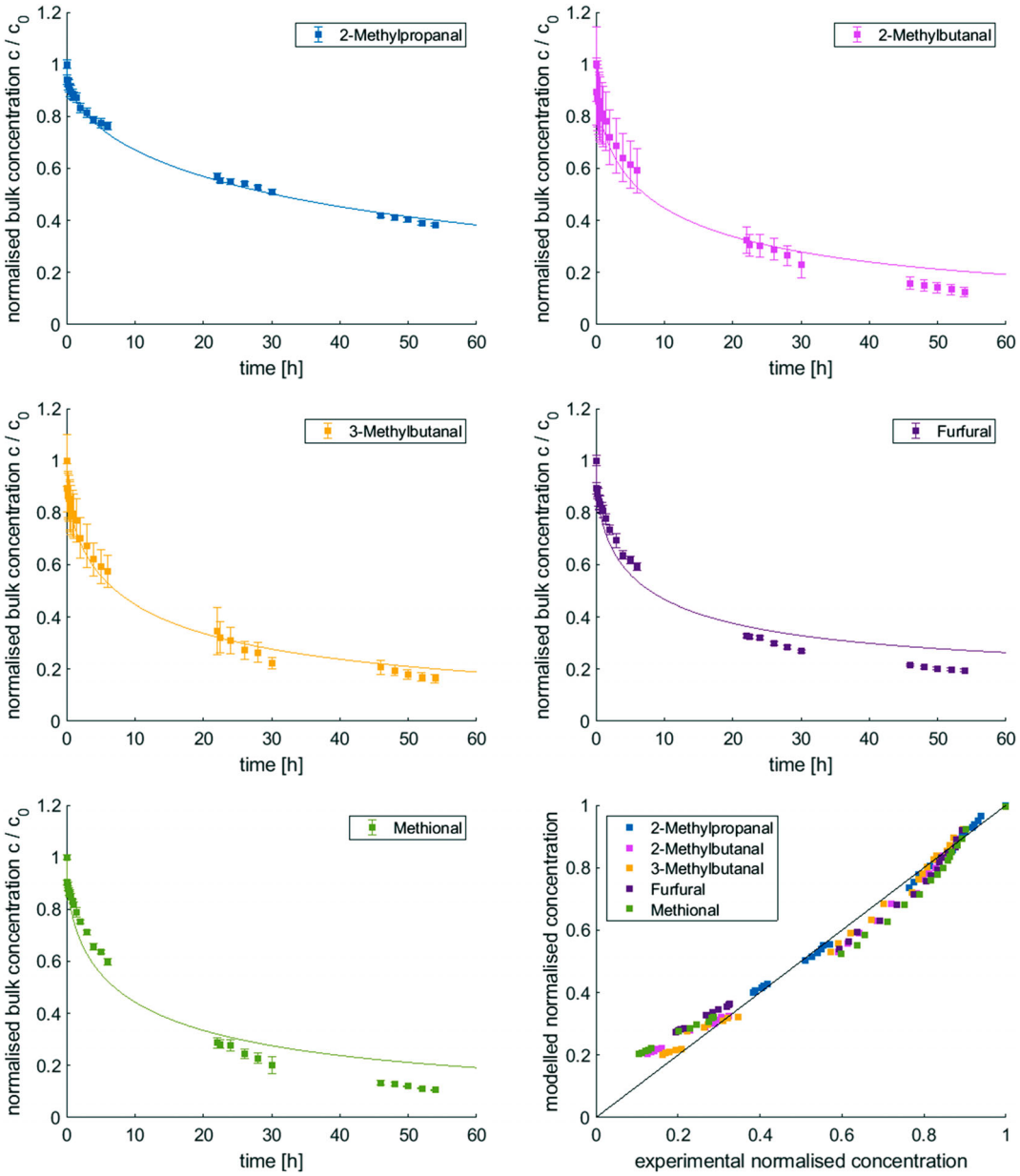

Figure 5 Experimental and model-based decrease of bulk concentration in model solution for 2-MP, 2-MB, 3-MB, FF, and Met for particles with a radius of 1.175 mm (small).

Investigating mass transfer in model solution

In this section, the experimental data of uptake experiments is presented, and the effective diffusivity is regressed with the HSDM. Representative for all settings, Fig. 5 shows the uptake of 2-MP, 2-MB, 3-MB, FF, and Met from the model solution starting at 0.5 mg L^{-1} and $d_p = 2.35$ mm. From Fig. 5 we can observe that the uptake follows an asymptotic behaviour and is relatively similar in shape to 2-MB, 3-MB, Met, and FF, converging towards the equilibrium loading. Nonetheless, even after an experimental time of 54 h, the equilibrium state is not reached.

While, overall, the model describes the experimental data sufficiently well, a general trend of overestimating the initial diffusivity and underestimating it in the later stage is observed. This effect is emphasized in the parity plot of Fig. 5, showing a deviation from the predicted values in the lower range of concentrations. Contrary to other studied compounds, the uptake of 2-MP is very well described by the model ($R^2 = 0.99$). Remarkably, 2-MP follows a less pronounced decline, only reducing to 40% of its initial concentration in the bulk after 54 h, despite being the smallest molecule studied. This goes against the expectation that mass transfer is related to the molecular size.

The regressed effective diffusion coefficients, their average relative error (ARE), and the associated coefficient of determination (R^2) of all performed tests are listed in Table 2. At first glance, we can observe that the effective diffusivities are very small and range vastly from $1.6{\cdot}10^{-15}$ (3-MB) to $4.1{\cdot}10^{-13}$ (FF) $m^2\ s^{-1}$, which is nearly a factor 100 times difference. This range is comparable to literature values presented in Table 1. The coefficients of determination are >0.9, except for the medium sized granules. Here, the initial slope in the bulk concentration is even flatter, resulting in

Journal of Chemical Technology & Biotechnology published by John Wiley & Sons Ltd on behalf of Society of Chemical Industry.

Table 2 Regressed effective diffusion coefficient, associated error, average relative error and coefficient of determination

		2-MP				2-MB				3-MB			
d_p [mm]	C_0 [mg/L]	D_{eff} [m^2/s]	σ_{Deff} [m^2/s]	ARE [%]	R^2	D_{eff} [m^2/s]	σ_{Deff} [m^2/s]	ARE [%]	R^2	D_{eff} [m^2/s]	σ_{Deff} [m^2/s]	ARE [%]	R^2
2.35	0.5	$3.0\cdot10^{-14}$	$2.2\cdot10^{-15}$	2.0	0.99	$6.5\cdot10^{-15}$	$1.5\cdot10^{-15}$	13.4	0.98	$4.2\cdot10^{-15}$	$7.4\cdot10^{-16}$	6.5	0.98
2.656	0.5	$2.5\cdot10^{-14}$	$9.5\cdot10^{-15}$	5.4	0.87	$2.8\cdot10^{-15}$	$2.3\cdot10^{-15}$	15.4	0.75	$2.0\cdot10^{-15}$	$1.4\cdot10^{-15}$	14.5	0.80
3.118	0.5	$2.9\cdot10^{-14}$	$4.0\cdot10^{-15}$	1.7	0.98	$3.9\cdot10^{-15}$	$1.7\cdot10^{-15}$	11.2	0.91	$2.5\cdot10^{-15}$	$8.8\cdot10^{-16}$	11.2	0.93
2.35	0.25	$2.2\cdot10^{-14}$	$5.8\cdot10^{-15}$	3.2	0.95	$4.5\cdot10^{-15}$	$2.2\cdot10^{-15}$	9.4	0.93	$3.3\cdot10^{-15}$	$1.6\cdot10^{-15}$	8.2	0.93
2.35	0.125	$1.5\cdot10^{-14}$	$2.8\cdot10^{-15}$	1.6	0.97	$3.7\cdot10^{-15}$	$1.5\cdot10^{-15}$	8.7	0.95	$2.3\cdot10^{-15}$	$9.0\cdot10^{-16}$	7.2	0.95

		FF				Met			
d_p [mm]	C_0 [mg/L]	D_{eff} [m^2/s]	σ_{Deff} [m^2/s]	ARE [%]	R^2	D_{eff} [m^2/s]	σ_{Deff} [m^2/s]	ARE [%]	R^2
2.35	0.5	$4.1\cdot10^{-13}$	$1.2\cdot10^{-13}$	13.0	0.97	$3.8\cdot10^{-14}$	$1.2\cdot10^{-14}$	22.4	0.96
2.656	0.5	$2.9\cdot10^{-13}$	$9.5\cdot10^{-14}$	4.1	0.95	$2.3\cdot10^{-14}$	$1.1\cdot10^{-14}$	14.3	0.90
3.118	0.5	$2.4\cdot10^{-13}$	$7.6\cdot10^{-14}$	2.4	0.95	$2.5\cdot10^{-14}$	$9.6\cdot10^{-15}$	7.2	0.93
2.35	0.25	$1.7\cdot10^{-13}$	$4.8\cdot10^{-14}$	3.0	0.96	$1.8\cdot10^{-14}$	$9.0\cdot10^{-15}$	6.9	0.92
2.35	0.125	$7.9\cdot10^{-14}$	$2.5\cdot10^{-14}$	5.3	0.95	$1.4\cdot10^{-14}$	$4.7\cdot10^{-15}$	8.2	0.96

a lesser fit with the model. Although the experiment was carried out in duplicate, this might be related to non-optimal flow conditions resulting in additional resistance to the mass transfer. The ARE is reasonable, ranging between 2–15% and the model is, hence, able to predict the mass transfer phenomena. Only methional's diffusivity in the small granules shows a larger ARE, which is due to the higher deviation of the predicted and experimental concentrations as described above at $c_i << c_0$.

Implication of results

In addition to the quantitative analysis of the mass transfer to regress diffusivities, the results were analysed qualitatively to understand what the most dominant transport mechanism is and where the highest resistance lies. Considering the order of magnitude of the regressed effective diffusivities, the relatively large granule size, and the high interstitial velocity, intraparticle mass transport is supposedly the controlling step during the adsorption process. This is confirmed when calculating the respective Biot numbers (Eqn (17)), which are presented in Table 3. A Biot number $>>10$ indicates mass transfer controlled through intraparticle diffusion, while $1 < Bi < 10$ marks a transitional regime where both external and intraparticle mass transfer determine the adsorption process. In our case, intraparticle transport is indeed limiting ($Bi >> 10$). In the case of furfural at $c_0 = 0.5$ mg L^{-1} and dp = 2.35 and 2.66 mm, the Biot number is found between 10 and 100, meaning that at lower flow rates, film diffusion may eventually become dominant.

$$Bi = \frac{k_f r_p c_0}{D_{eff} \rho_p q_{eq}(c_0)} \tag{17}$$

When regarding the intraparticle mass transfer, particularly in composite pellets and granules, macro−/meso-pore and micropore (*i.e.* intracrystalline) diffusivities can be differentiated. Both resistances can be limiting to the mass transport, depending on the ratio of the diffusional time constants $(D_{micro}/r_c^2)/(D_{macro}/r_p^2)$. Varying the particle size during experimental uptake tests is hence a way of understanding the bottleneck of the transport path.[31] Figure 6 shows the relation of the regressed effective diffusivities of all studied compounds to the initial concentration and the particle size, respectively.

From the figure, it appears that increasing the initial concentration slightly increases the diffusion coefficient and that the diffusivity slightly decreases with increasing particle diameter. However, due to the error associated with the regression, no significant statement can be made. From the regressed experimental data, it is not clear whether the diffusivity in the transport macropores or in the micropores of the zeolite crystals is limiting. A thorough study of recent literature also reveals that beside macro- or micropore limitations also other effects, such as surface barriers at the crystal surface[34, 35, 47] can

Table 3 Calculated Biot numbers for all conditions

		Biot number []				
d_p [mm]	C_0 [mg L^{-1}]	2-MP	2-MB	3-MB	FF	Met
2.35	0.5	435	420	529	55	182
2.656	0.5	555	1037	1180	82	320
3.118	0.5	519	806	1023	108	319
2.35	0.25	425	501	551	112	310
2.35	0.125	447	504	648	205	321

Journal of Chemical Technology & Biotechnology published by John Wiley & Sons Ltd on behalf of Society of Chemical Industry.

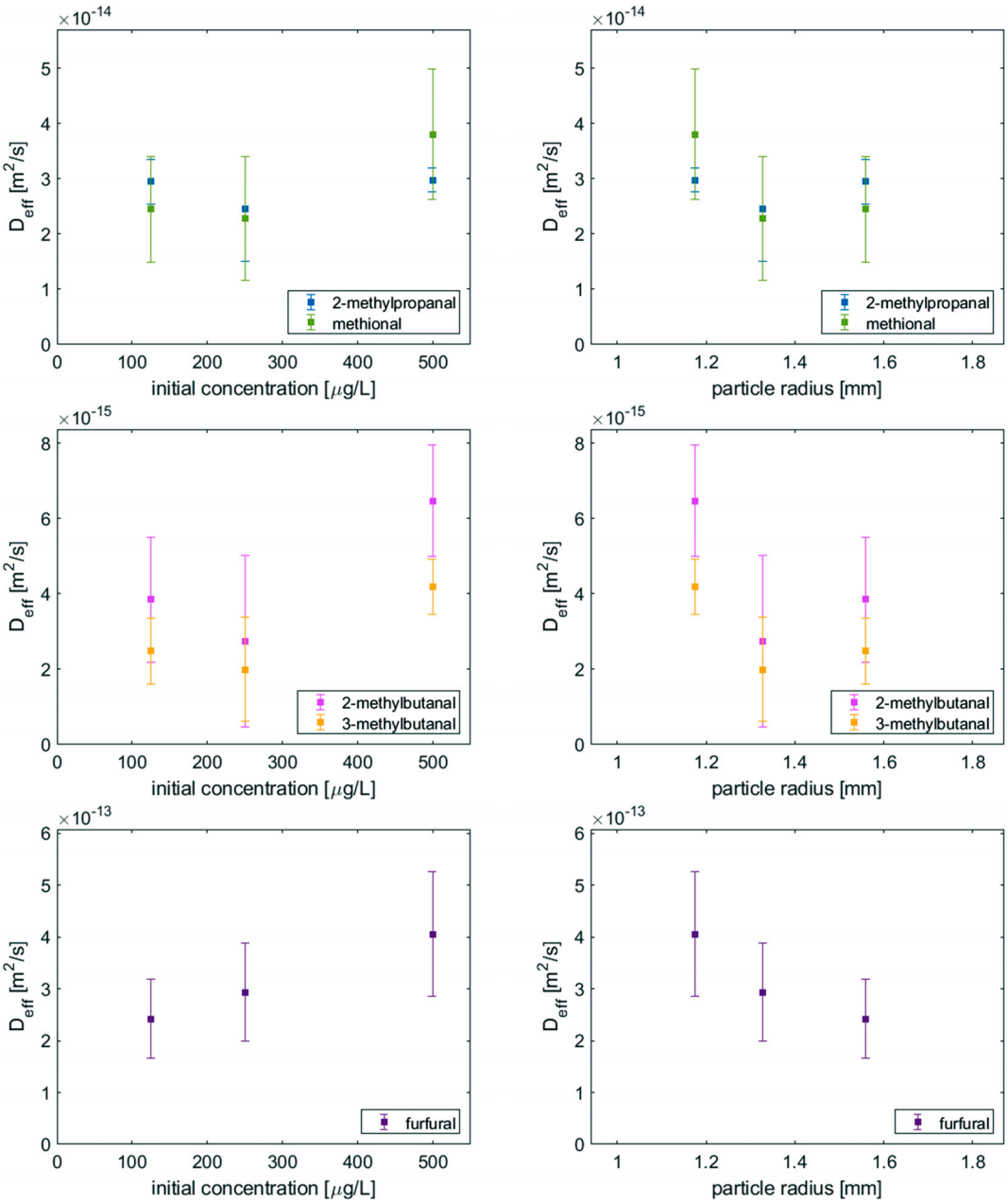

Figure 6 Regressed effective diffusion coefficient *versus* initial bulk concentration (left) and particle radius (right).

be involved, making a straight-forward analysis of the time-constants difficult. Other factors such as distribution in crystal size or agglomeration of these may also influence the results.[34]

The effect of the concentration, depicted in Fig. 6, is also important with regard to the assumption of a non-competitive adsorption process. If vacant adsorption sites would be limiting, the diffusivity should be lower at the higher initial concentration. Hence, we conclude that the separate analysis of compounds holds.

As mentioned above, neither a correlation between the molecular weight and the diffusivity nor a correlation between the molecular radius and the diffusion coefficients could be made. A tentative relation between increasing molecular volume and decreasing effective diffusivity can be suggested, as shown in Fig. 7. However, there is a remarkable correlation between the hydrophobicity (represented by the logD value) and, hence, the adsorbent affinity constant with the diffusivity. That is, the more hydrophobic a compound and the higher its affinity to the adsorbent, the slower the transport through the particle. When considering Eqn (18),[23] the effect of the adsorption affinity constant on the overall intraparticle mass transfer coefficient can be understood. Thus, this observation could be interpreted as a manifestation of (macro)pore diffusion being the controlling mechanism, as the characteristic time of the macropore mass transfer is proportional to the affinity constant K(c).

$$\frac{1}{k_{intra,eff}} = \frac{K(c)r_p^2}{15\varepsilon D_p} + \frac{r_c^2}{15D_c} \tag{18}$$

Alternatively, the dependency on the affinity constant could be related to intracrystalline diffusion controlling the mass transfer.

Journal of Chemical Technology & Biotechnology published by John Wiley & Sons Ltd on behalf of Society of Chemical Industry.

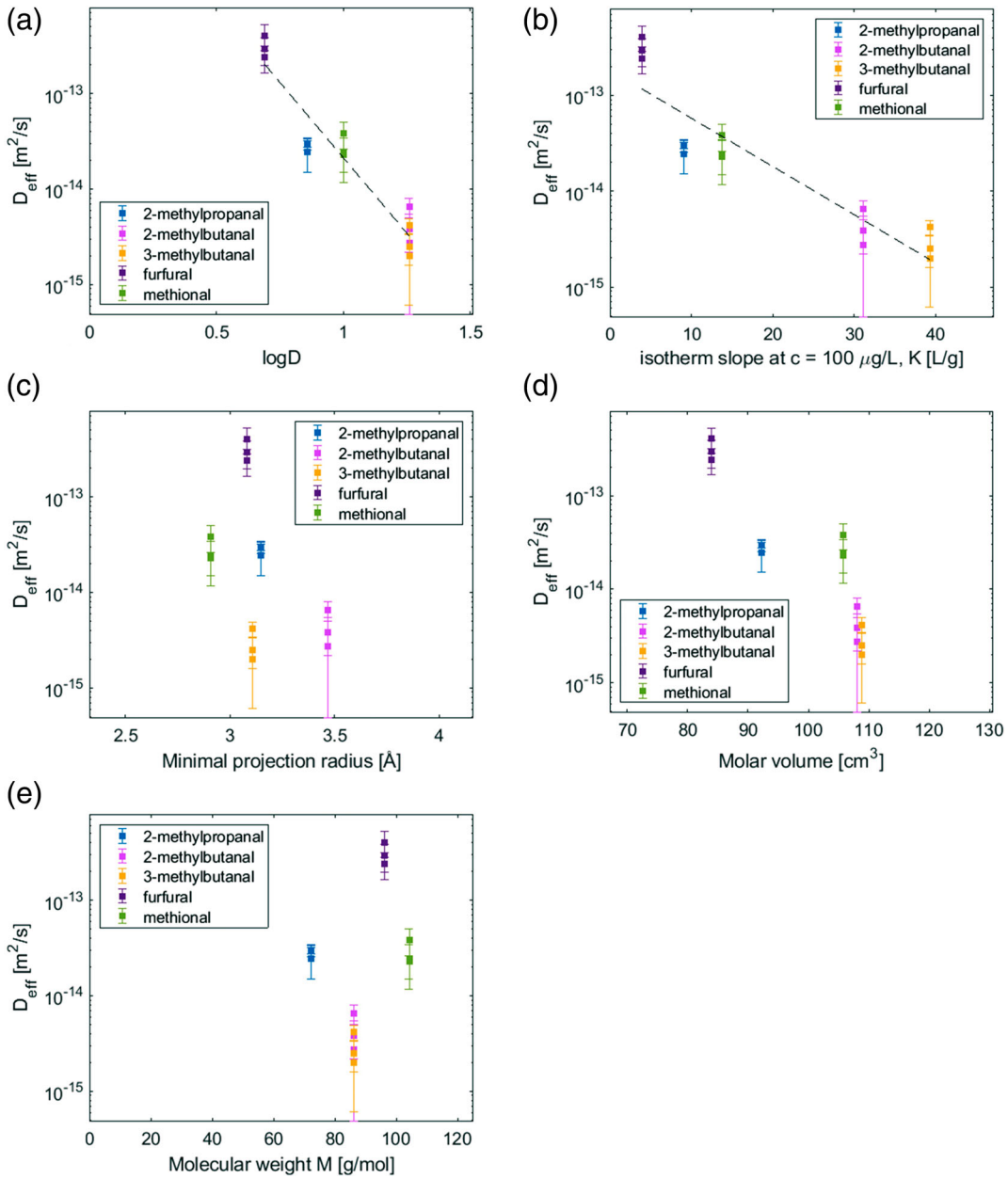

Figure 7 Correlation of regressed effective diffusion coefficient to (a) the molecular hydrophobicity (expressed as logD) and (b) the isotherm affinity constant as well as (c) is the minimal projection radius, (d) the molar volume and (e) the molecular weight.

A similar relation on the adsorbent affinity constant was reported by Wach *et al.* (2018) for sugar molecules on hydrophobic Y-zeolite.[23] The authors of the study concluded that a higher adsorbent affinity results in a slowed diffusion though the micropores, *i.e.* decreased intracrystalline diffusivity. Another systematic study of non-volatile phenolic compounds' diffusion in zeolite beta and silicalite crystals was performed by Linh *et al.* (2016). Also, in their case, the adsorption affinity rather than the critical diameter of the adsorbate was correlated to the intracrystalline diffusivity.[48] This mechanism resembles that of surface diffusion, which is limited by the adsorption energy of the sample. The migration of strongly adsorbing compounds is hence restricted by the adsorbate-adsorbent-interaction.[49, 50]

Since the resistances in macro- and micropores are additive, it is probable that both macropore diffusion and intracrystalline diffusion play a major role in our case. Moreover, in Fig. 5, it was observed that the model fit resulted in an overestimation of the diffusivity in the initial stage of the uptake and an underestimation at higher adsorbent loading, when the equilibrium state was nearly reached. Overall, a logic explanation for the observed behaviour could be similar to the following: Initially, the adsorbate has to overcome the surface barrier posed by the outer shell of the granule. It then diffuses along the macropore system, while at the same time, the adsorbate begins to penetrate the surface and micropores of the (agglomerated) crystals, which poses an additional transport resistance. After the adsorbate has fully penetrated the macropores of the granule, the uptake rate solely depends on the micropore diffusivity. Since the full volume of the granule is now filled with adsorbate, the uptake appears faster than in the beginning. The effect of varying particle size could therefore become much less sharp. Surely, other effects, such as

Journal of Chemical Technology & Biotechnology published by John Wiley & Sons Ltd on behalf of Society of Chemical Industry.

the agglomeration of crystals and the resulting variation of the micropore resistance, may play a role as well.

Even though the actual mass transfer mechanism remains hypothetical, some conclusions for improving the material can be drawn. Decreasing the particle size of the granule itself, but also the crystals (*i.e.* reduce crystal agglomerated sizes), would be an effective measure to accelerate the mass transfer. However, also increasing the overall proportion of the transport pores would be beneficial to accelerate the mass transfer through the particle. This could, for instance, also mean introducing hierarchical structures into the zeolite crystals themselves in the form of mesopores.[51]

Knowing these limitations, a sophisticated process unit design will help to increase the productivity despite the mass transfer limitations. Both the choice of a superior material (shape) and the process conduct must be optimized in order to make the selective wort flavour removal feasible. Thereby, it is important to find a trade-off between fast mass transfer, which would be best in a powder shaped adsorbent, and regenerability and practical handling, where shaped zeolites are advantageous. A conceptual process design will give further insight into the optimal solution for this case.

CONCLUSIONS

In this study, the mass transfer of five flavour compounds in binder-free, hydrophobic ZSM-5 granules was investigated. The characterization of the material indicated that the granule consists of small crystals connected by macropores of 180 nm and shaped into the bigger granule, which is surrounded by a denser outer layer or shell for mechanical stability. We found that the porosity calculated from gravimetrical experiments with ethanol were most representative of the accessible pore volume for small organic molecules, including the void in intracrystalline micropores. Following this, the equilibrium of the multicomponent model solution was studied to obtain the adsorption isotherms described by the Freundlich model. Due to the near linear shape of the isotherms, it was concluded that the adsorption process is non-competitive and, hence, the behaviour of the single compounds can be studied independently in the multicomponent solution.

Subsequently, during hydrodynamically well-defined batch uptake experiments, the dynamics of the adsorption process were measured, and the effective diffusivities were obtained by applying the HSDM. The diffusivities ranged in the order of magnitude of 10^{-13}- 15^{-15} m^2 s^{-1}. The HSDM was suitable to regress the effective diffusion coefficient but it showed some deviation at the asymptotic area of the uptake curve. Because of the relatively high associated error of the diffusivities, there was no clear impact of a varying particle diameter or a concentration effect visible. Furthermore, there was no obvious correlation of the diffusivity with molecular size or weight. Yet, a strong correlation between the intraparticle diffusion and the hydrophobicity and, hence, the affinity of the compound to the adsorbent material, was found. While this data is useful to model and design a unit operation to remove such flavour from liquid food streams, the exact mass transfer mechanism remains hypothetical. Most likely, the transport through the pores, in combination with a high resistance in the intracrystalline micropores, form the bottleneck in the mass transfer process.

In conclusion, we recommend the development of materials that have a more optimal particle and crystal size distribution for liquid adsorption and/or a higher proportion of transport meso- and macropores to ensure fast uptake of the target compounds and transport to the micropores. It is possible that high-end analytical techniques, such as micro-imaging[47] or NMR studies,[31] could help to elucidate the actual mechanism inside the granule. Many of these, however, are not applicable to liquids at such low concentrations and small crystal sizes. For future work, it would be interesting to verify if the correlation of diffusivity and hydrophobicity also holds for other materials (shapes) and molecule groups. Furthermore, a conceptual process design study will reveal the feasibility of the process at a commercial scale.

ACKNOWLEDGEMENTS

We gratefully acknowledge Heineken Supply Chain B.V. for funding this project. Furthermore, we would like to thank Dr. C. Bläker (Universität Duisburg-Essen) and Dr. A. Fletcher (University Strathclyde) for carrying out the sorption experiments for the material characterization, as well as Dr. D. Hartig (Technische Universität Braunschweig) for taking the SEM pictures. We would also like to thank and Dr. P. van den Broeke for his feedback and Dr. C. Picioreanu (Delft University of Technology) for his contribution to the computational work.

REFERENCES

1 Chmelik C and Kärger J, In situ study on molecular diffusion phenomena in nanoporous catalytic solids. *Chem Soc Rev* **39**:4864–4884 (2010).
2 Hwang S and Kärger J, NMR diffusometry with guest molecules in nanoporous materials. *Magn Reson Imaging* **56**:3–13 (2019).
3 Kärger J and Ruthven DM, Diffusion in nanoporous materials: fundamental principles, insights and challenges. *New J Chem* **40**: 4027–4048 (2016).
4 Krishna R, The Maxwell-Stefan description of mixture diffusion in nanoporous crystalline materials. *Micropor Mesopor Mat* **185**:30–50 (2014).
5 Babel S and Kurniawan TA, Low-cost adsorbents for heavy metals uptake from contaminated water: a review. *J Hazard Mater* **97**: 219–243 (2003).
6 Erdem E, Karapinar N and Donat R, The removal of heavy metal cations by natural zeolites. *J Colloid Interface Sci* **280**:309–314 (2004).
7 Wang S and Peng Y, Natural zeolites as effective adsorbents in water and wastewater treatment. *Chem Eng J* **156**:11–24 (2010).
8 Moliner M, Román-Leshkov Y and Davis ME, Tin-containing zeolites are highly active catalysts for the isomerization of glucose in water. *Proc Natl Acad Sci U S A* **107**:6164–6168 (2010).
9 Holm MS, Saravanamurugan S and Taarning E, Conversion of sugars to lactic acid derivatives using heterogeneous Zeotype catalysts. *Science* **328**:602–605 (2010).
10 Berensmeier S and Buchholz K, Separation of isomaltose from high sugar concentrated enzyme reaction mixture by dealuminated *β*-zeolite. *Sep Purif Technol* **38**:129–138 (2004).
11 Wach W, Fornefett I, Buttersack C and Buchholz K, Chromatographic separation of saccharide mixtures on zeolites. *Food Bioprod Process* **114**:286–297 (2019).
12 Ching CB, Ho C, Hidajat K and Ruthven DM, Experimental study of a simulated counter-current adsorption system-V. comparison of resin and zeolite absorbents for fructose-glucose separation at high concentration. *Chem Eng Sci* **42**:2547–2555 (1987).
13 Sánchez ÓJ and Cardona CA, Trends in biotechnological production of fuel ethanol from different feedstocks. *Bioresour Technol* **99**: 5270–5295 (2008).
14 Taarning E, Osmundsen CM, Yang X, Voss B, Andersen SI and Christensen CH, Zeolite-catalyzed biomass conversion to fuels and chemicals. *Energy Environ Sci* **4**:793–804 (2011).
15 Gernat DC, Penning MM, Swinkels FM, Brouwer ER and Ottens M, Selective off-flavor reduction by adsorption: a case study in alcohol-free beer. *Food Bioprod Process* **121**:91–104 (2020).
16 Beal AD and Mottram DS, Compounds contributing to the characteristic aroma of malted barley. *J Agric Food Chem* **42**:2880–2884 (1994).
17 Perpète P and Collin S, Contribution of 3-methylthiopropionaldehyde to the worty flavor of alcohol-free beers. *J Agric Food Chem* **47**: 2374–2378 (1999).

Journal of Chemical Technology & Biotechnology published by John Wiley & Sons Ltd on behalf of Society of Chemical Industry.

18 Meilgaard MC, *Flavor Chemistry in Beer: Part II: flavor and Flavor Threshold of 239 Aroma Volatiles*, Vol. **12**. Master Brewers Association of the Americas, pp. 151–168 (1975).
19 Andrés-Iglesias C, Nešpor J, Karabín M, Montero O, Blanco CA and Dostálek P, Comparison of carbonyl profiles from Czech and Spanish lagers: traditional and modern technology. *LWT - Food Sci Technol* **66**:390–397 (2016).
20 Holtkamp M and Scholl S, Adsorption properties of BEA zeolites and their aluminum phosphate extrudates for purification of isomaltose. *Adsorption* **17**:801–811 (2011).
21 García MG, García Fernández JM and Buttersack C, Adsorption of difructose dianhydrides on hydrophobic Y-zeolites. *Microporous Mesoporous Mater* **292**:109673 (2020).
22 Fornefett I, Rabet D, Buttersack C and Buchholz K, Correction adsorption of sucrose on zeolites [Green Chem (2016) 18 (3378–3388) DOI: 10.1039/C5GC02832A]. *Green Chem* **20**:3643 (2018).
23 Wach W, Buttersack C and Buchholz K, Chromatography of mono- and disaccharides on granulated pellets of hydrophobic zeolites. *J Chromatogr A* **1576**:101–112 (2018).
24 Buttersack C, Rudolph H, Mahrholz J and Buchholz K, High specific interaction of polymers with the pores of hydrophobic zeolites. *Langmuir* **12**:3101–3106 (1996).
25 Waluga T and Scholl S, Process design aspects for reaction-integrated adsorption in multi-enzymatic catalysis. *Chem Eng Technol* **38**: 1817–1826 (2015).
26 Ching CB and Ruthven DM, A liquid phase chromatographic study of sorption and diffusion of glucose and fructose in NaX and KX zeolite crystals. *Zeolites* **8**:68–73 (1988).
27 Ma YH and Lin YS eds, *Adsorption and Diffusion of Liquids in Silicalite using HPLC*. American Institute of Chemical Engineers Symposium Series, National Meeting, 259 ed., pp. 1–10 (1987).
28 Vidal CB, Raulino GSC, Da Luz AD, Da Luz C, Do Nascimento RF and De Keukeleire D, Experimental and theoretical approach to multicomponent adsorption of selected aromatics on hydrophobically modified zeolite. *J Chem Eng Data* **59**:282–288 (2014).
29 Ching CB and Ruthven DM, Sorption and diffusion of some amino acids in KX zeolite crystals. *Chem Eng J* **40**:B1–B5 (1989).
30 Guiochon G, *Fundamentals of Preparative and Nonlinear Chromatography*, 2nd edn. Elsevier, Boston, MA (2006).
31 J Kärger DMR. *Diffusion in Zeolites and Other Microporous Solids*. New York: Wiley & Sons INC; 605 p. (1992).
32 Choi JG, Do DD and Do HD, Surface diffusion of adsorbed molecules in porous media: monolayer, multilayer, and capillary condensation regimes. *Ind Eng Chem Res* **40**:4005–4031 (2001).
33 Kärger J, Pfeifer H, Richter R, Fürtig H, Roscher W and Seidel R, NMR study of mass transfer in granulated molecular sieves. *AIChE J* **34**: 1185–1189 (1988).
34 Rao SM, Saraçi E, Gläser R and Coppens MO, Surface barriers as dominant mechanism to transport limitations in hierarchically structured catalysts – application to the zeolite-catalyzed alkylation of benzene with ethylene. *Chem Eng J* **329**:45–55 (2017).
35 Teixeira AR, Chang CC, Coogan T, Kendall R, Fan W and Dauenhauer PJ, Dominance of surface barriers in molecular transport through Silicalite-1. *J Phys Chem C* **117**:25545–25555 (2013).
36 Wilke CR and Chang P, Correlation of diffusion coefficients in dilute solutions. *AIChE J* **1**:264–270 (1955).
37 Bird RB, Stewart WE and Lightfoot EN, *Transport Phenomena*, 2nd edn. Wiley International, New York, NY (2002).
38 Weber TW and Chakravorti RK, Pore and solid diffusion models for fixed-bed adsorbers. *AIChE J* **20**:228–238 (1974).
39 Rosen JB, Kinetics of a fixed bed system for solid diffusion into spherical particles. *J Chem Phys* **20**:387–394 (1952).
40 Ijzer AC, Vriezekolk E, Dekic Zivkovic T and Nijmeijer K, Adsorption kinetics of DowexTM OptiporeTM L493 for the removal of the furan 5-hydroxymethylfurfural from sugar. *J Chem Technol Biotechnol* **91**: 96–104 (2016).
41 Skoog DA, Holler FJ and Crouch SR, *Principles of Instrumental Analysis*, 6th edn. Thomson-Brooks/Cole, Belmont, CA (2007).
42 Brunauer S, Emmett PH and Teller E, Adsorption of gases in multimolecular layers. *J Am Chem Soc* **60**:309–319 (1938).
43 ISO. 15901–1: 2016, *Evaluation of Pore Size Distribution and Porosity of Solid Materials by Mercury Porosimetry and Gas Adsorption - Part 1: Mercury Porosimetry*, p. 19 (2016).
44 Vesely P, Lusk L, Basarova G, Seabrooks J and Ryder D, Analysis of aldehydes in beer using solid-phase microextraction with on-fiber derivatization and gas chromatography/mass spectrometry. *J Agric Food Chem* **51**:6941–6944 (2003).
45 Advanced Chemistry Development IAL. ACD/Percepta Platform Toronto, ON, Canada: ACD/Labs; 2019 [2018.1]: Available from: www.acdlabs.com.
46 Galarneau A, Villemot F, Rodriguez J, Fajula F and Coasne B, Validity of the t-plot method to assess microporosity in hierarchical micro/mesoporous materials. *Langmuir* **30**:13266–13274 (2014). [28 August 2019].
47 Remi JCS, Lauerer A, Chmelik C, Vandendael I, Terryn H, Baron GV *et al*., The role of crystal diversity in understanding mass transfer in nanoporous materials. *Nat Mater* **15**:401–406 (2016).
48 Linh TN, Fujita H and Sakoda A, Diffusion of non-volatile phenolic compounds in zeolite beta and silicalite in liquid phase. *Adsorption* **22**: 1001–1011 (2016).
49 Miyabe K and Guiochon G, Surface diffusion in reversed-phase liquid chromatography. *J Chromatogr A* **1217**:1713–1734 (2010).
50 Miyabe K and Guiochon G, Correlation between surface diffusion and molecular diffusion in reversed-phase liquid chromatography. *J Phys Chem B* **105**:9202–9209 (2001).
51 Groen JC, Zhu W, Brouwer S, Huynink SJ, Kapteijn F, Moulijn JA *et al*., Direct demonstration of enhanced diffusion in mesoporous ZSM-5 zeolite obtained via controlled desilication. *J Am Chem Soc* **129**: 355–360 (2007).
52 Breck DW, *Zeolite Molecular Sieves: Structure, Chemistry and Use*. JWS Technologies, Inc, New York, NY (1974).

APPENDICES

MEASUREMENT OF PORE SIZE DISTRIBUTION

Figures 8–10 depict the adsorption and desorption isotherm of nitrogen and mercury as well as the resulting pore size distribution, respectively.

EQUILIBRIUM BATCH UPTAKE EXPERIMENTS

Table 4 summarized all tested conditions to obtain the adsorption equilibrium.

DETERMINATION OF VISCOSITY AND CHOICE OF MODEL SOLUTION COMPOSITION

The viscosity at various shear rates was measured with a rolling-ball viscometer (LOVIS 2000 ME, Anton Paar, Austria) according to the procedures recommended by the manufacturer. Figure 11 shows the viscosity of various maltodextrin solutions in dependency of the shear rate. Furthermore, the viscoelastic behaviour of alcohol-free beer (AFB) was analysed. Hence, it was found that a maltodextrin solution of 65 g L^{-1} mimics the viscosity of AFB best.

INVESTIGATION OF HYDRODYNAMIC CONDITIONS DURING UPTAKE EXPERIMENTS

In Fig. 12, a preliminary experiment was performed with the model solution containing only furfural ($c_0 = 9$ mg L^{-1}) to ensure that the flow rate does not affect the uptake dynamics during the ZGC measurement. Despite some variance in the measurements, there is no statistically significant difference between the uptake experiments at different flow rates and also no trend can be observed. It is hence concluded, that at the chosen conditions (flowrate 60 mL min^{-1}), the effect of the intraparticular transport is isolated and can be obserced indepedently from the effect of film mass transfer or external diffusion limitations, *i.e.* the bulk is ideally mixed.

Journal of Chemical Technology & Biotechnology published by John Wiley & Sons Ltd on behalf of Society of Chemical Industry.

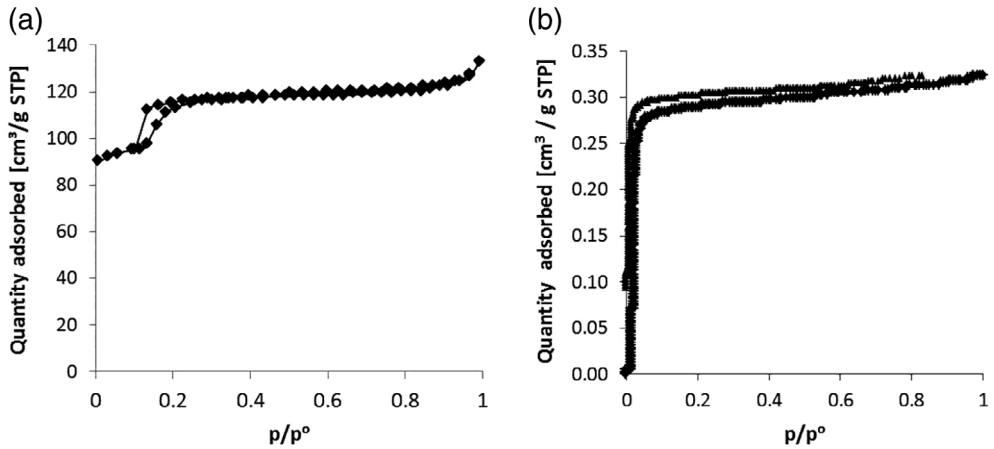

Figure 8 Adsorption / desorption isotherm of ZSM-5 G-360 of (a) nitrogen and (b) mercury.

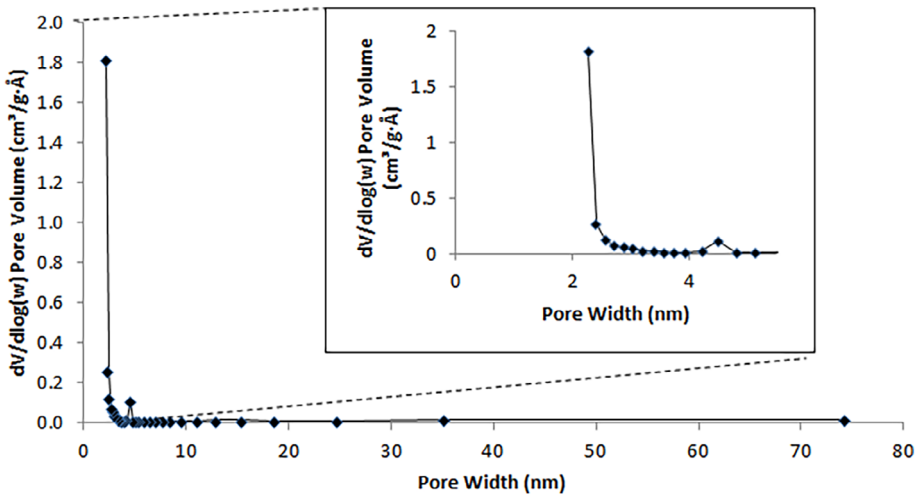

Figure 9 Pore size distribution of ZSM-5 G-360 resulting from BET measurement with nitrogen.

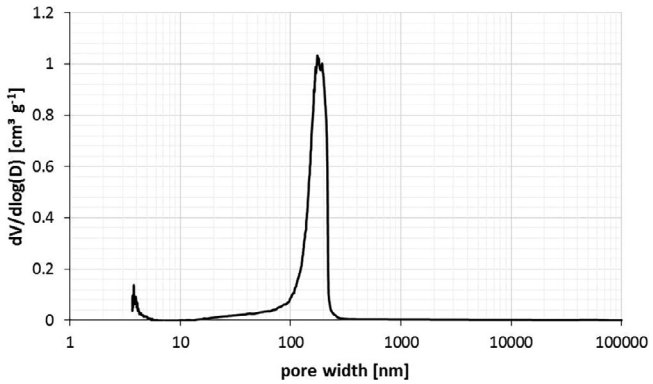

Figure 10 Pore size distribution of ZSM-5 G-360 resulting from sorption measurement with mercury.

Journal of Chemical Technology & Biotechnology published by John Wiley & Sons Ltd on behalf of Society of Chemical Industry.

Table 4 Overview on selected batch uptake experiments to determine the isotherm

#	Phase ratio [kg_{liq}/g_{ads}]	c_i [mg/kg_{liq}]
1	2.0	$c_{2\text{-MP}} = 1.425$
2	1.5	$c_{2\text{-MB}} = 1.540$
3	1.0	$c_{3\text{-MB}} = 1.280$
		$c_{FF} = 1.521$
		$c_{Met} = 1.700$
4	1.0	$c_{2\text{-MP}} = 2.849$
		$c_{2\text{-MB}} = 3.081$
		$c_{3\text{-MB}} = 2.560$
		$c_{FF} = 3.042$
		$c_{Met} = 3.397$
5	1.0	$c_{2\text{-MP}} = 5.698$
		$c_{2\text{-MB}} = 6.161$
		$c_{3\text{-MB}} = 5.120$
		$c_{FF} = 6.084$
		$c_{Met} = 6.793$
6	1.0	$c_{2\text{-MP}} = 11.396$
		$c_{2\text{-MB}} = 12.322$
		$c_{3\text{-MB}} = 10.240$
		$c_{FF} = 12.168$
		$c_{Met} = 13.586$

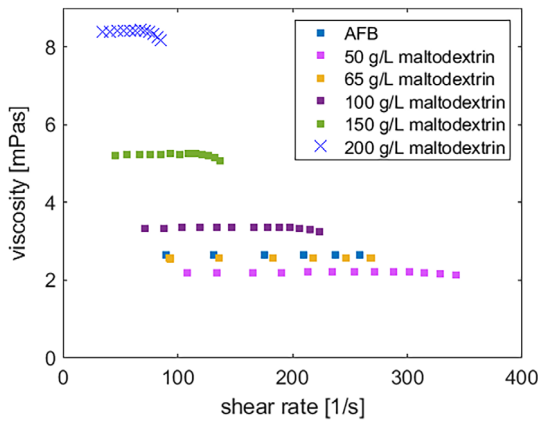

Figure 11 Viscosity of various maltodextrin solutions at pH 4.2 and alcohol-free beer in dependency of the shear rate.

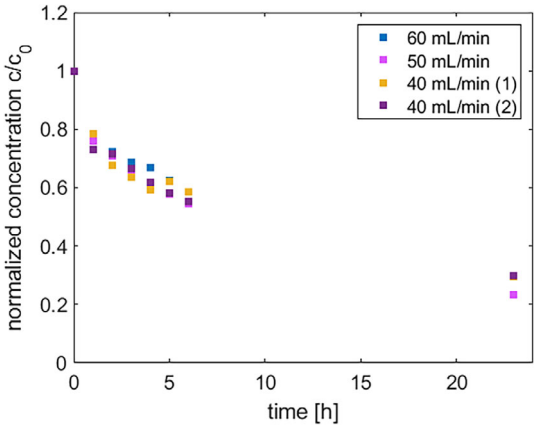

Figure 12 Uptake of furfural at different flow rates over the hydrodynamically defined batch uptake experiment.

Journal of Chemical Technology & Biotechnology published by John Wiley & Sons Ltd on behalf of Society of Chemical Industry.